energies

MDPI

Article

Power Quality Improvement with Three-Phase Shunt Active Power Filter Prototype Based on Harmonic Component Separation Method with Low-Pass Filter

Marian Gaiceanu *, Silviu Epure, Razvan Constantin Solea and Razvan Buhosu

Faculty of Automation, Computers, Electrical Engineering and Electronics, Dunarea de Jos University of Galati, 800008 Galati, Romania; silviu.epure@ugal.ro (S.E.); razvan.solea@ugal.ro (R.C.S.); razvan.buhosu@ugal.ro (R.B.)
* Correspondence: marian.gaiceanu@ugal.ro

Abstract: This work contributes to both Romania's and the European Union's energy policies by highlighting the research results obtained within the Dunarea de Jos University of Galati, but also through the technological transfer of this knowledge to the industry. In order to improve the power quality of the nonlinear loads connected to the electrical grid, a three-phase shunt active power filter prototype based on the Harmonic Component Separation Method with a Low-Pass Filter was used. The active power filter is connected at the Point of Common Coupling to compensate for individual loads or even all of them simultaneously. Therefore, active power filters can be used to compensate for the power factor and reduce the harmonic distortion of power supplies, or for processes subsequently connected to additional nonlinear loads, thus improving the energy efficiency. The shunt active power filter prototype is composed of the power side (three-phase insulated gate bipolar transistor bridge, DC link capacitor precharge system, inductive filter) and the control side (gate drive circuits, control subsystems, signal acquisition system). The filter control strategy is based on the principle of separating harmonic components with a low-pass filter, implemented by the authors on the industrial prototype. In this paper, the main technical features of the industrial shunt active power filter prototype are specified. The authors of this paper involved three cascaded control loops: the DC link voltage control loop, the shunt active power filter current control loop and the phase-locked loop. Both simulation and experimental results for the shunt-type active power filter prototype were obtained. By analyzing the obtained waveforms of the power supply source in two cases (with and without an active power filter), a decrease in the total harmonic distortion was demonstrated, both the voltage harmonic distortion factor THDu and the current harmonic distortion factor THDi in the case of the active power filter connection. By using the Field-Programmed Gate Array processing platform, the powerful computational speed features were exploited to implement the active shunt power filter control on an experimental test bench. Conducting source current harmonics mitigation increased the efficiency of the power system by decreasing the respective harmonic Joule losses. The energy-saving feature led to the increased added value of the parallel active power filter. Through the performed laboratory tests, the authors demonstrated the feasibility of the proposed control solution for the industrial prototype. In accordance with the European Union's Research and Technological Development Policy, the development of an innovation ecosystem was taken into consideration. The unified and efficient integration of all the specific actors (enterprises, research institutes, universities and entrepreneurs) in innovation was achieved.

Keywords: shunt active power filter; prototype; compensation strategy; harmonic component separation method; low-pass filter; energy efficiency; sustainability; THDu; THDi

check for updates

Academic Editors: Frede Blaabjerg and Ahmed Abu-Siada

Received: 18 November 2024
Revised: 3 January 2025
Accepted: 5 January 2025
Published: 24 January 2025

Citation: Gaiceanu, M.; Epure, S.; Solea, R.C.; Buhosu, R. Power Quality Improvement with Three-Phase Shunt Active Power Filter Prototype Based on Harmonic Component Separation Method with Low-Pass Filter. *Energies* **2025**, *18*, 556. https://doi.org/10.3390/en18030556

Copyright: © 2025 by the authors. Licensee MDPI, Basel, Switzerland. This article is an open access article distributed under the terms and conditions of the Creative Commons Attribution (CC BY) license (https://creativecommons.org/licenses/by/4.0/).

1. Introduction

The global energy demand has begun to rise, leading to greater energy production [1]. Most of the increased demand will come from investments in renewable energy sources, energy conservation and energy savings [2–4]. Unfortunately, most energy-saving [5–8] electrical equipment has the side effect of drawing a current in a non-sinusoidal fashion, known as current harmonic distortion [9–13]. The resulting harmonic currents lead to the following disadvantages: increased energy consumption, increased system losses, an increased demand on power equipment and increased distortions in the electrical grid. The problem of a distorted current is that it affects the voltage waveform, leading to distortions in the supply voltage, in which case all the equipment supplied from the grid will operate under abnormal conditions and thus deviate from their normal behaviour. This leads to limitations on the power supply and use of the electrical grid, the premature ageing of products, higher losses, vibration at the motor shaft, production stoppages and increased electromagnetic interference [14,15]. Thus, harmonics reduce reliability, affect the product quality, increase operating costs and cause decreased productivity. The harmonic contamination of electrical energy distribution systems, generated by power electronic equipment, has led researchers to look for solutions to reduce these harmonics. In industrial settings, household appliances and transport units, there are variable speed drive systems based on voltage source PWM inverters having a three-phase diode rectifier as the front-end power converter [16]. This solution is very widespread due to its simplicity, high efficiency, low cost and high reliability. The main disadvantage of these non-controlled (diode) rectifiers is the generation of high amounts of harmonic currents, affecting compliance with existing harmonic standards [17]. For harmonic mitigation [18,19], different solutions have been proposed, divided into passive or active filters [20]. The disadvantages of passive filters are as follows: they are bulky with a fixed harmonic mitigation capability; the resonance phenomenon can occur at fundamental and all harmonic orders. Depending on the objectives, the current and voltage harmonics compensation could be mitigated by using a dc or ac APF. From a system configuration point of view, there are series, shunt and hybrid APFs. According to [20], from a harmonic detection point of view, the developed methods are load current detection, supply current detection and voltage detection. From a power rating point of view, APFs are divided into current-fed PWM inverters (high rating power) and voltage-fed PWM inverters. In this paper, a three-phase voltage-fed shunt active power filter prototype based on the load current detection method was studied. A low-pass filter (LPF) passes only low-frequency signals, and it was used to obtain the DC component of the input signal. Consequently, the LPF eliminates all the critical harmonic frequencies above or equal to the resonating frequency [21,22].

This paper is divided into five sections. In the Introduction Section, the importance of the power quality issue is highlighted, along with its mitigation methods. The Materials and Methods Section specifies the technical parameters of the SAPF prototype and the generic power structure of it. The Generation of the SAPF Current References Section contains the mathematical model of the SAPF prototype used and details of the Harmonic Component Separation Method with a Low-Pass Filter (HCSLPF) used to synthesize the current references of the SAPF. In the Results Section, both the simulation and the experimental results obtained by the authors on the SAPF prototype are presented. The main features of the research results are highlighted in the Conclusions Section.

2. Materials and Methods

The main parameters of the SAPF prototype, resulting from the design stage, are presented in Table 1.

Table 1. Main technical parameters of the SAPF.

Parameters		Technical Data	
Rated voltage		400 V ± 10% [V]	
Nominal frequency		50 [Hz]	
Rated current		25 [A]	
Number of phases		3 phases + PE	
Degree of protection		IP21	
Cooling method		Forced cooling	
Compliance with standards		EN IEC 61000-6-2 [23], EN IEC 61000-6-4 [24], EN 50178 [25]	
Control method		LabView FPGA, Harmonic Component Separation Method with low-pass filter—HCSLPF	
Communication interface		ETHERNET; RS 232; RS 485; CAN; USB	
Harmonic range		1–50 (50–2500 Hz/50 Hz)	
Dimensions (L × W × H), mm		1200 × 300 × 1000	
Climatic conditions	Ambient temperature	Relative humidity	Atmospheric pressure
Operation	5–40 °C	5–85%	86–106 kPA
Storage	−25–55 °C	5–95%	86–106 kPA
Transport	−25–70 °C	95%	70–106 kPA

In Figure 1, the power structure of the experimental test bench is depicted. The power system consists of the SAPF connected at the Point of Common Coupling in parallel with the nonlinear load and national grid. The power structure of the SAPF is based on a three-phase voltage inverter, in which the gate control signals (G1–G6) are delivered according to the Harmonic Component Separation Method with a Low-Pass Filter (HCSLPF). Through the adequate measurement of the DC voltage across the capacitor, grid power supply currents, load currents and APF currents, the control side generates six pulses according to Figure 1. The industrial electric oven supplied by a nonlinear power converter was considered in this study [1].

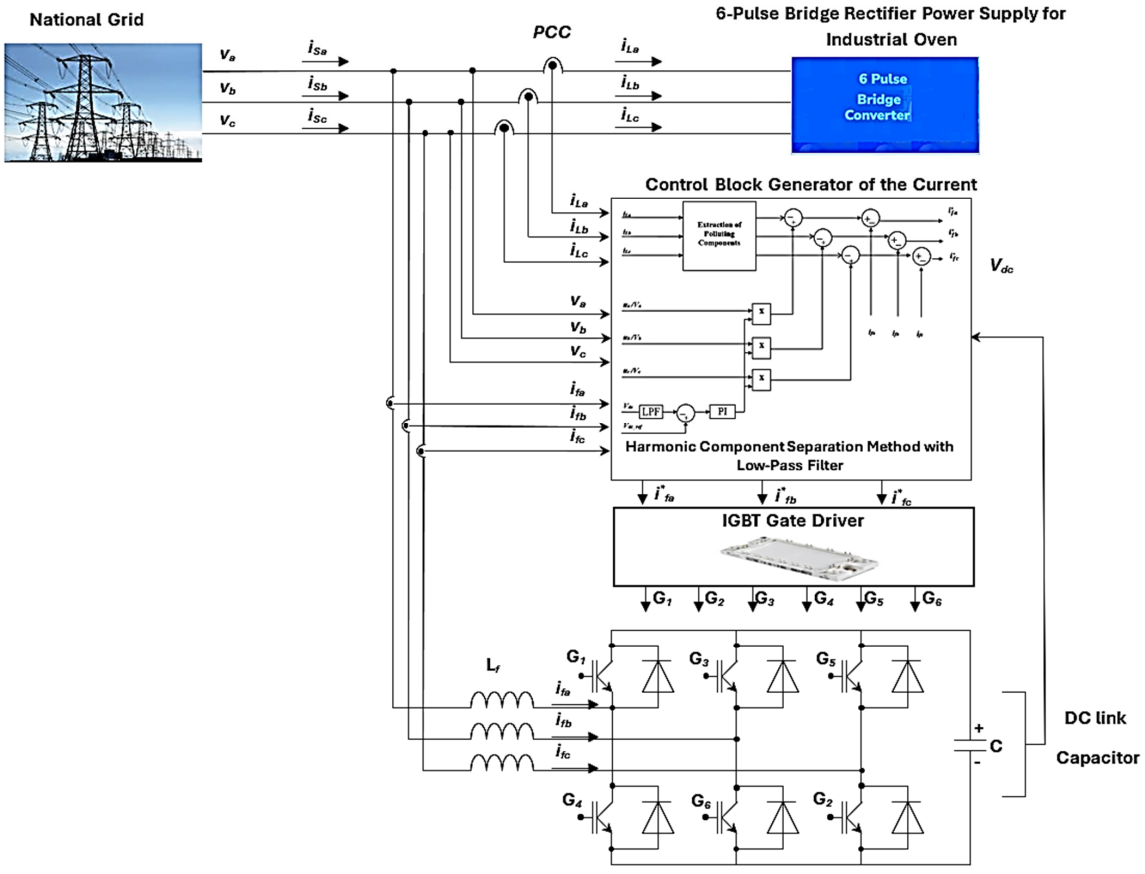


Figure 1. The Harmonic Component Separation Method with a Low-Pass Filter.

The equivalent power system developed in MATLAB-Simulink R2017a is presented in Figure 2. In order to implement the developed model concept (Figure 1), the DC link capacitor's pre-charging phase through the delayed SAPF operational connection (Figure 2) was taken into account.

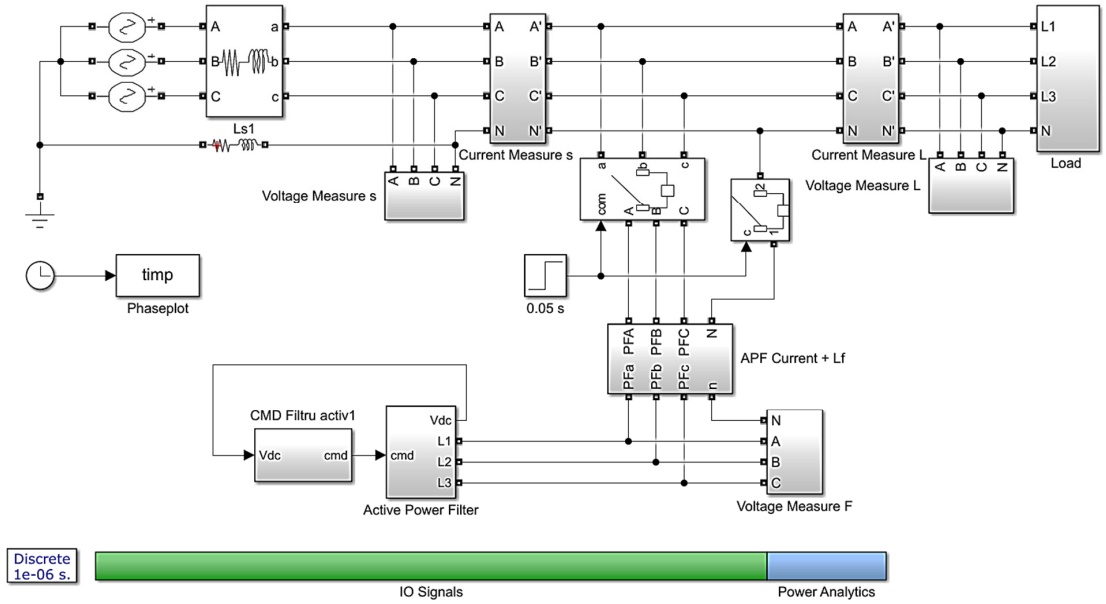


Figure 2. The MATLAB-Simulink implementation of the harmonic improvement power system (HCSLPF).

3. Generation of the SAPF Current References

According to Figure 1, at the Point of Common Coupling (PCC), for one phase, the instantaneous currents are related according to Kirchhoff's first law:

$$i_{sa}(t) = i_{La}(t) + i_{fa}(t) \tag{1}$$

where i_{sa} is the instantaneous power supply current, i_{La} is the instantaneous load current and i_{fa} is the instantaneous filter current.

At the same time, the instantaneous active power of the power supply is made up of that of the fundamental active component (P_S) and the harmonic component ($\widetilde{p}_S$).

$$p_s = P_s + \widetilde{p}_s, \tag{2}$$

or at the level of the instantaneous power,

$$p_s = p_L + p_f. \tag{3}$$

The same analysis from a reactive power point of view provides the instantaneous form:

$$q_s = Q_s + \widetilde{q}_s, \tag{4}$$

and

$$q_s = q_L + q_f. \tag{5}$$

Therefore, if the pollutant (or harmonic) component of the power supply vanishes, $\widetilde{p}_S = 0$, the following condition is obtained:

$$\widetilde{p}_f = -\widetilde{p}_L. \tag{6}$$

By using the adequate physical quantities for one phase, the harmonic current of the SAPF is obtained:

$$\tilde{\iota}_{fa} = -\tilde{\iota}_{La}. \tag{7}$$

The fundamental of the active power is the ratio

$$P_f = \frac{\Delta W_s}{T}, \tag{8}$$

between ΔW_s (the capacitive energy variation) and T (the sample period of the supply voltage). The capacitive energy is stored in the DC link capacitor.

By extracting the load current harmonics from the power supply harmonic currents, the reference currents for the SAPF are obtained [22]:

$$i^*_{fa} = \frac{P_f}{3V_a}\sqrt{2}sin\omega t - \tilde{\iota}_{La}, \tag{9}$$

$$i^*_{fb} = \frac{P_f}{3V_b}\sqrt{2}sin\left(\omega t - \frac{2\pi}{3}\right) - \tilde{\iota}_{Lb}, \tag{10}$$

$$i^*_{fc} = \frac{P_f}{3V_c}\sqrt{2}sin\left(\omega t - \frac{4\pi}{3}\right) - \tilde{\iota}_{Lc} \tag{11}$$

In Figure 3, the generation principle of the SAPF current references to compensate for the harmonics content is presented.

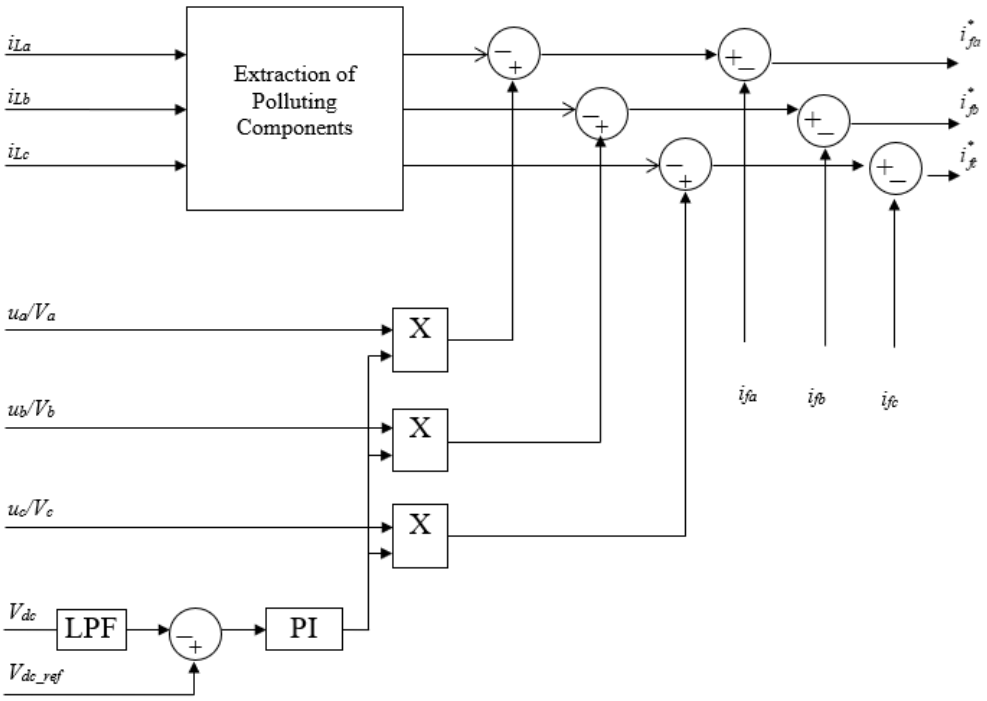


Figure 3. Block diagram of the generation of current references for the active power filter using Harmonic Component Extraction.

The SAPF current references are delivered based on the LPF harmonics extraction method (Figure 3) from the load currents, with the three-phase APF measurements acting as feedback signals in the SAPF current loops (Figure 4). In Figure 4, the DC link capacitor voltage control loop based on a PI regulator is shown. The voltage control was designated to maintain a constant average DC voltage on the DC capacitor, smoothing the voltage variation and delivering the reference for the fundamental active power (P_f) of the APF. By

using Equations (9)–(11), the reference currents for the SAPF are obtained. The hysteresis current modulator provides both the current control and appropriate switching states for the three-phase voltage power bridge.

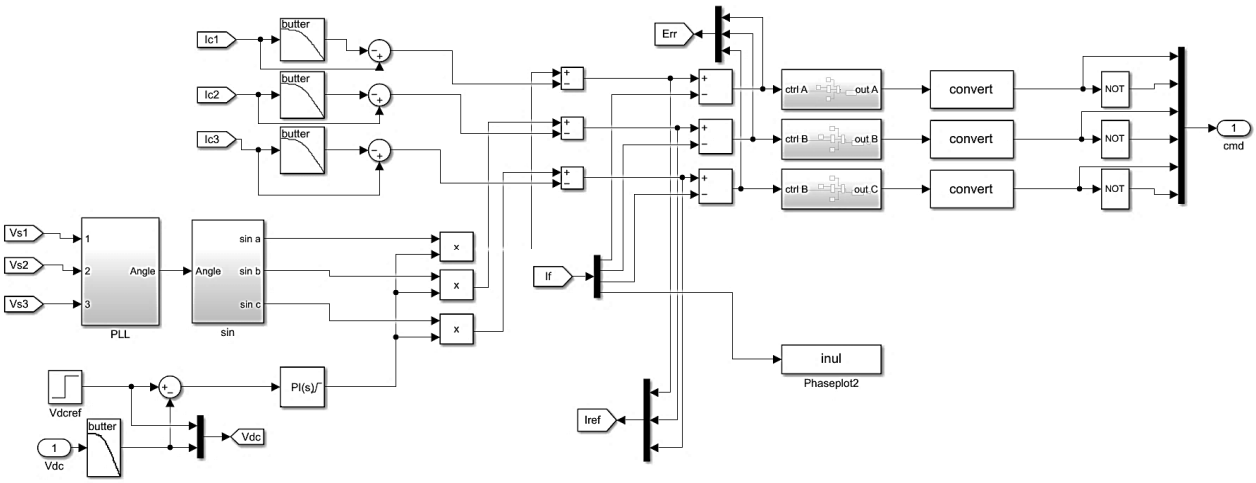


Figure 4. The MATLAB-Simulink implementation of the harmonic improvement control system by using the HCSLPF control method.

In Figure 3, the SAPF current references are shown. In Figure 4, the HCSLPF SAPF control, as well as the filter current three-phase references to compensate for the harmonics content, is depicted. The user-defined blocks in Figures 2 and 4 are based both on the control principle of the detailed Harmonic Component Separation Method with a Low-Pass Filter shown in Figure 1 and on the block diagram of the SAPF current reference generation (Figure 3).

The control loops of the SAPF are arranged in a cascaded manner: the outer loop is the DC link voltage loop to maintain a constant DC link voltage, while the inner loops consist of the three-phase and individual-phase current loops to provide sinusoidal AC source currents, synchronized with the grid frequency via the PLL synchronization loop. The current control loops compare the APF current references with the APF feedback current (I_f), providing the switching states in the three-phase active power filter (Figure 4).

4. Results

The numerical simulation results from the SAPF using the HCSLPF control method are presented in this section, as well as the experimental results.

4.1. Numerical Simulation Results

The operation of the voltage control loop was validated through numerical simulations. In Figure 5, both the precharge operations and the normal operation of the SAPF are shown. The DC voltage reference for the precharge stage was established as 560 V, t = 0.05 s (Figure 5). At t = 0.35 s, the rated DC voltage (690 V) was applied as a reference (the blue line in Figure 5) and the SAPF was connected to the power system. The measured DC voltage is depicted in Figure 5 (red line). A zero steady-state error was obtained in the normal operation stage, with the feedback DC voltage smoothly reaching the reference. The proportional integral control was used.

A solution with a DC link precharge without additional components was used. In this case (Figure 5), using only the incorporated modulator in the power inverter was necessary [26,27]. The solid-state relay technology was based on the fast-switching MOSFET semiconductor device due to its fast transition times (rise and fall), high efficiency (low drain–source resistance during the conduction mode) and use of a noncomplex gate drive [28]. This method allowed us to remove the classical precharge circuit formed by the

precharge contactor and resistor, increasing both the efficiency and reliability. At the same time, the precharge time was significantly reduced compared to the classical precharge method. However, due to the PWM cycle time, the proper design of the cooling circuit was mandatory. This method allowed us both to control the inrush current and to decrease the precharge time. The solid-state technology used fits well with the industrial applications due to the high reliability in spite of the environmental conditions and mechanical shocks.

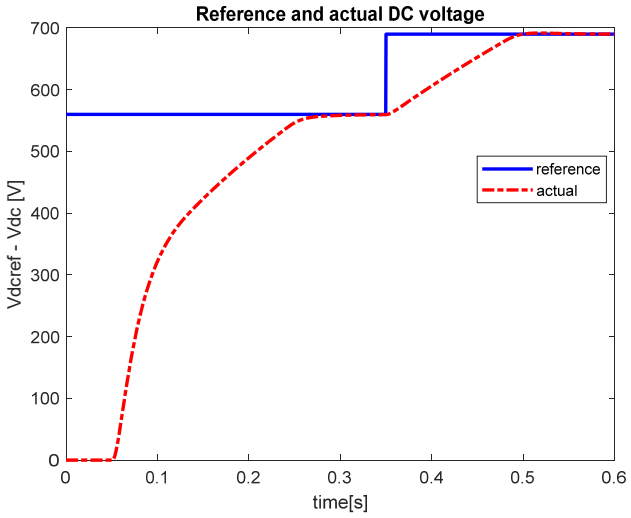


Figure 5. The operation of the DC voltage loop of the SAPF.

For the current control loop, in order to maintain a quasi-constant modulation frequency, the adaptive hysteresis band technique [29] was employed and adapted to the proposed HCSLPF control. The generated bandwidths' profiles (HB_a, HB_b, HB_c) depended on the DC link capacitor voltage, the reference current gradient, the supply voltage and the coupling inductor [30]. The inputs of the three-phase bandwidth's profile consisted of the filter current errors. The appropriate pulses were generated and delivered to the power filter.

Both the power supply voltage and the current are presented in Figure 6. It should be noted that in the absence of the SAPF ($0 < t < 0.05$ s), the phase current of the power supply was similar to the load current, being a strong distorted waveform. As a nonlinear load, the six-pulse bridge rectifier was used. With the SAPF connection, the harmonic content of the source current was diminished such that the phase source current became sinusoidal, like the phase voltage supply (Figure 6).

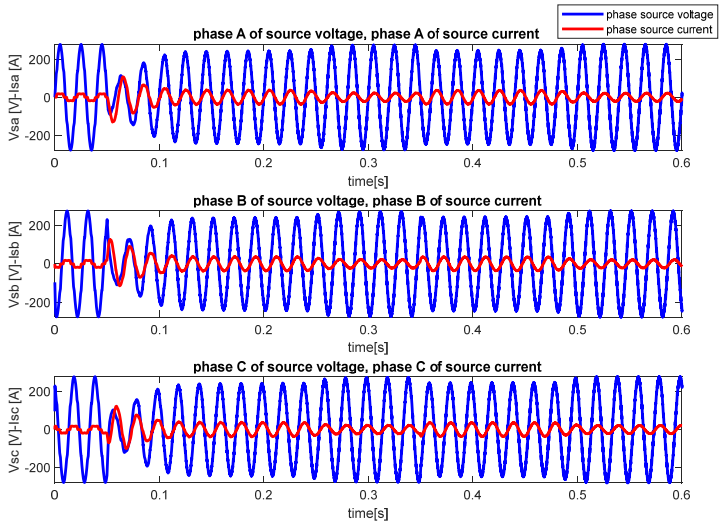


Figure 6. The power supply waveforms: three phase voltages (blue) and three phase currents (red).

The three-phase load (consumer) currents were nonlinear, as depicted in Figure 7.

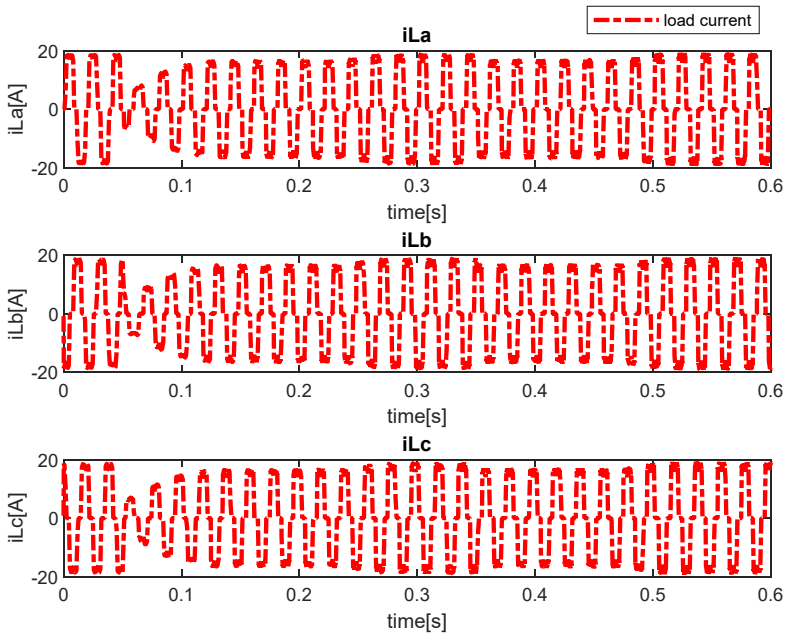


Figure 7. The nonlinear three-phase load currents.

The applied Harmonic Component Separation Method with a Low-Pass Filter affected the three-phase reference currents as in Figure 8.

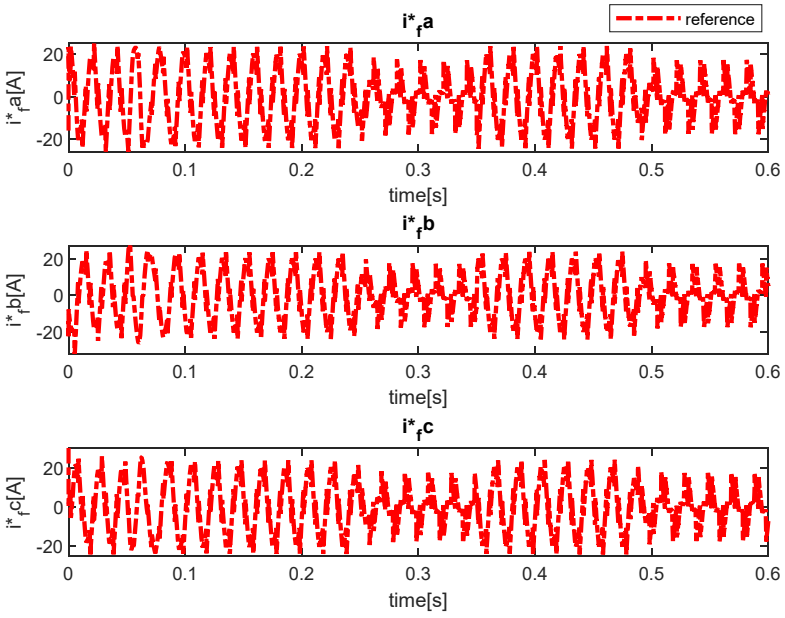


Figure 8. The three-phase reference currents generated by the HCSLPF.

In Figure 9, the three-phase SAPF feedback currents are shown. In both the operation modes (OFF—SAPF disconnected; ON—SAPF connected) of the power system, FFT current waveform analyses were performed. In the OFF operation mode (the disconnected SAPF), for the FFT analysis of the power supply phase current, the window of the first two cycles was selected (highlighted in a red colour in Figure 10).

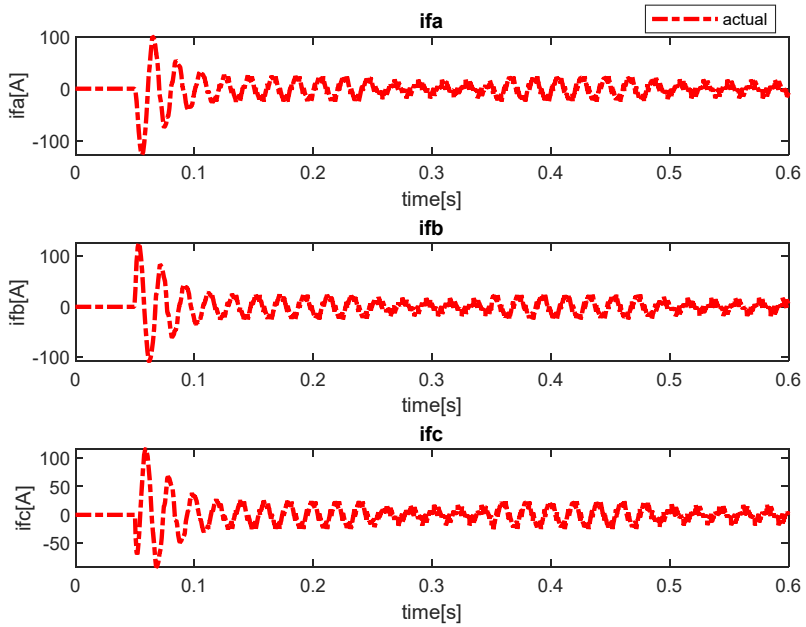


Figure 9. The measured three-phase SAPF currents.

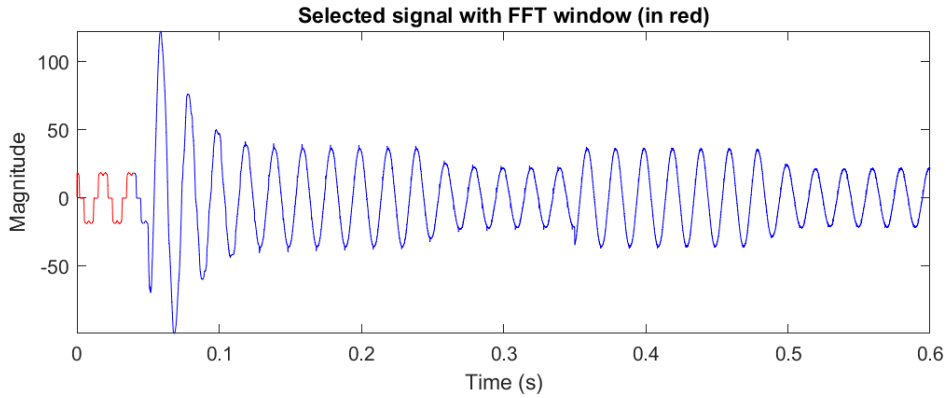


Figure 10. The selected FFT window (red line) from the power supply phase current analysis (blue line) without an SAPF connection (red marked signal).

In Figure 11, the FFT analyses reveal a total harmonic distortion of the power supply phase current of THD_I = 27.7%.

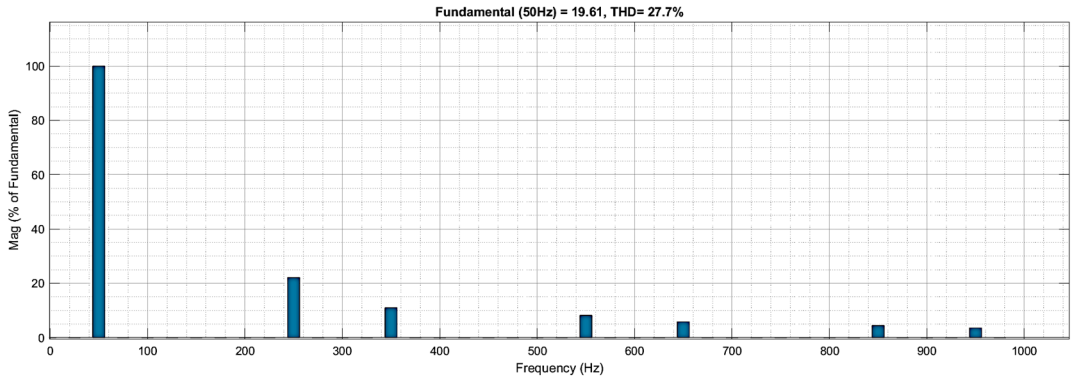


Figure 11. The FFT analyses of the power supply phase current without an SAPF connection.

In the ON operation mode (a connected SAPF system), for the FFT analysis of the power supply phase current, a window with two cycles was selected (highlighted in a red colour in Figure 12) at t = 0.55 s.

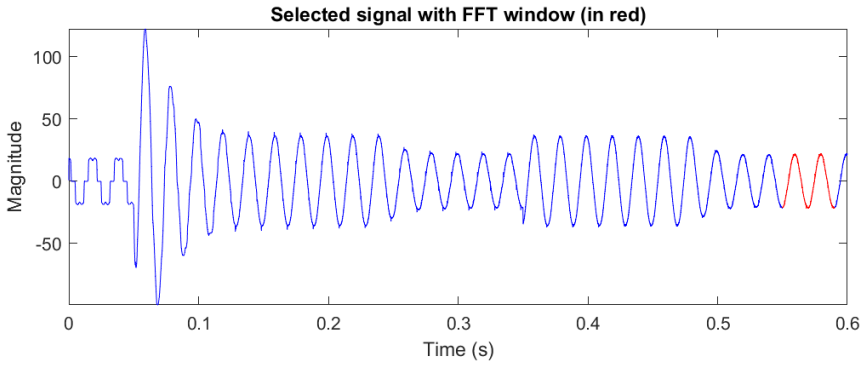


Figure 12. The selected FFT window (red line) from the power supply phase current (blue line) analysis with an SAPF connection (red marked signal).

In Figure 13, the FFT analyses reveal an improving THD factor of THD_I = 3.47%.

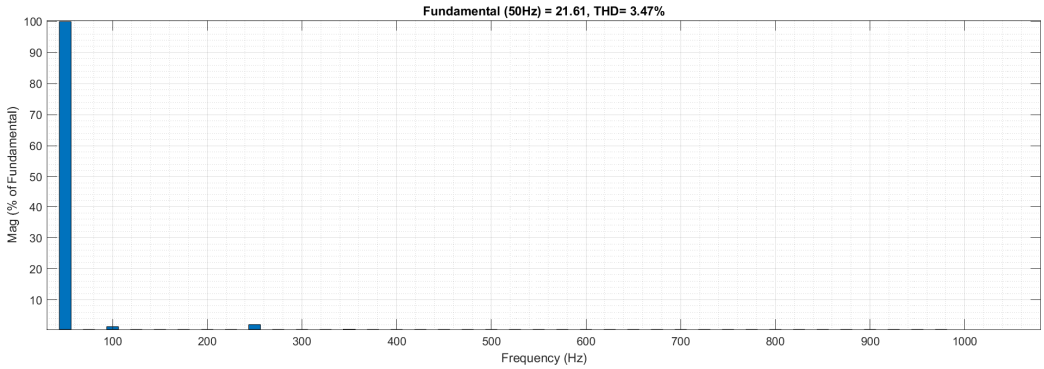


Figure 13. The FFT analyses of the power supply phas1 current with an SAPF connection.

To outline the THD improvement caused by using the Harmonic Component Separation Method with a Low-Pass Filter applied to the three-phase shunt active power filter prototype, a comparative side-by-side graphic is presented (Figure 14).

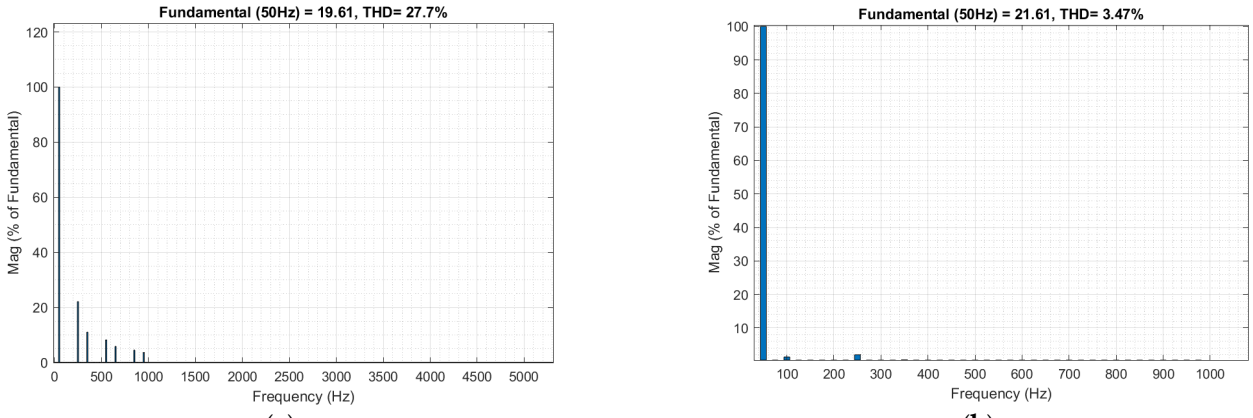


Figure 14. Comparative side-by-side THD analyses of the power supply phase current (**a**) without an SAPF connection and (**b**) with an SAPF connection.

According to the obtained simulation data, taking into consideration the 220 V supply phase voltage, by connecting it to the SAPF, the grid's current harmonic level distortion decreased from 27.7% (Figure 14a) to 3.47% (Figure 14b).

4.2. Experimental Results

Using the FPGA processing platform (cRIO-9039), the powerful calculus speed features were exploited to implement the SAPF control on an experimental test bench. In the PCC, voltage and current transducers were placed and located between the national grid source, load and SAPF. A standard PC was used to generate the programming file for the FPGA board to control and monitor the overall operation of the APF. The nonlinear load consisted of a three-phase six-bridge pulse rectifier supplying an electrical oven with 5 kW.

Inside the FPGA, the control loop of the APF contained the voltage and current scaling operations, low-pass filters, the PLL loop to generate sinusoidal reference voltages and the PWM generator (Figure 15).

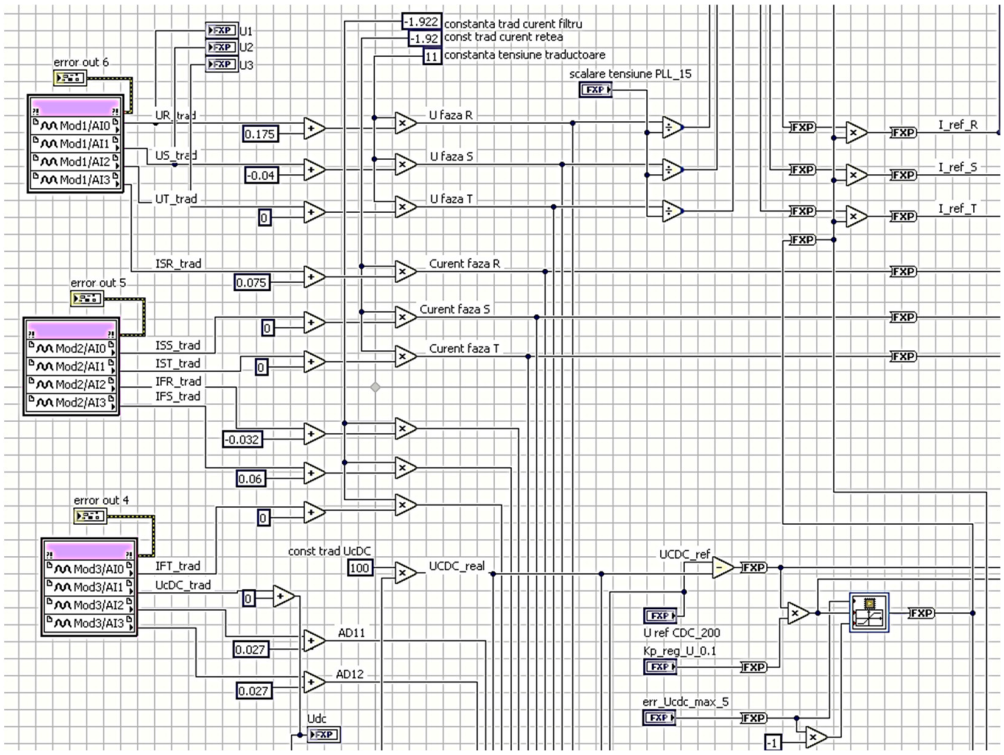


Figure 15. The FPGA control loop implementation of the SAPF industrial prototype.

The implemented PWM module generated complementary ON/OFF signals for the three arms of the power inverter (Figure 16). No dead time was implemented, since the IGBT driver already included this function as a standard protection. The PWM signal period was computed in FPGA "ticks", with a 15 kHz switching frequency meaning 3000 "ticks". This option allowed for fine PWM variations/increments of just 0.03%.

In Figure 17, the implemented FPGA PLL circuit is shown. The FPGA-implemented code contains the "Theta" constant, experimentally deducted. The phase synchronization of the output signals with the input waveforms was the main objective.

For the current loop, the sampling rate of the analogue signals was set to the 52 kHz. The current control loops had as inputs the current references compared with the real current signals. The outputs of the current control loops were the reference values to be sent to the PWM modulator.

The experimental data were obtained using the FLUKE 437 Series II Power Quality and Energy Analyzer, 400 Hz.

Figure 18 shows that the grid three-phase voltage supply was obtained from the Power Analyzer used. In the case of the nonlinear load, in Figure 19, comparative national grid voltage and current phasors are presented.

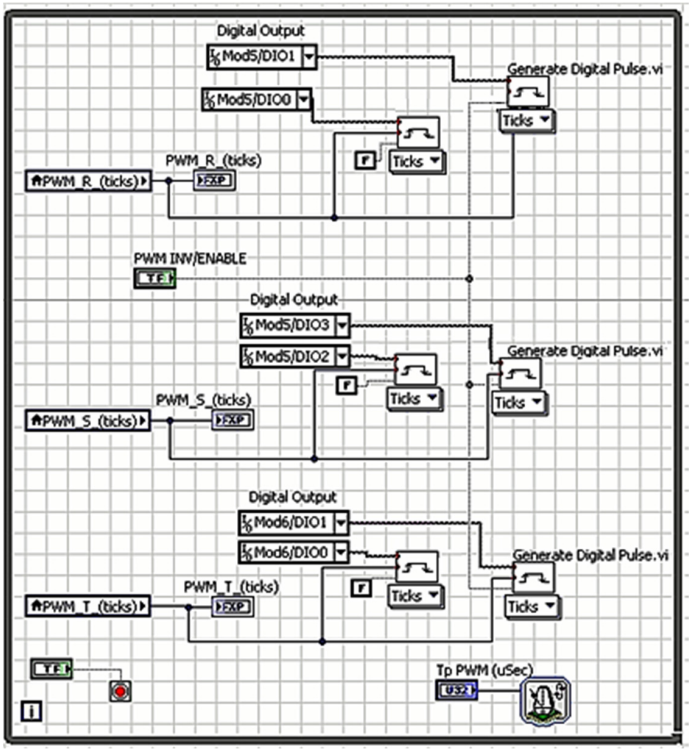


Figure 16. The implemented three-phase FPGA PWM signal generator.

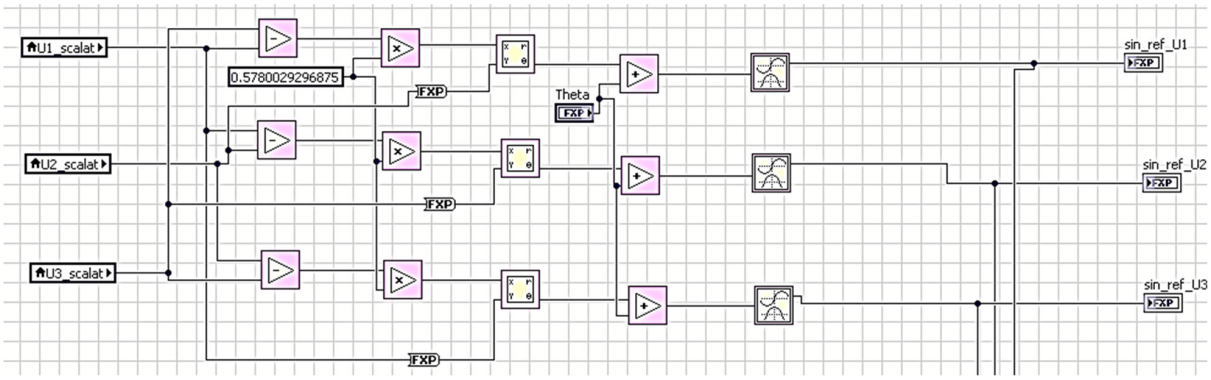


Figure 17. The implemented FPGA PLL circuit.

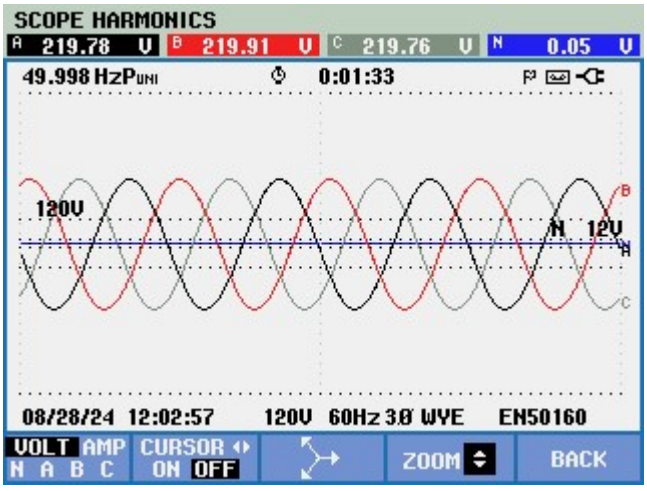


Figure 18. The grid three-phase voltage with a nonlinear load.

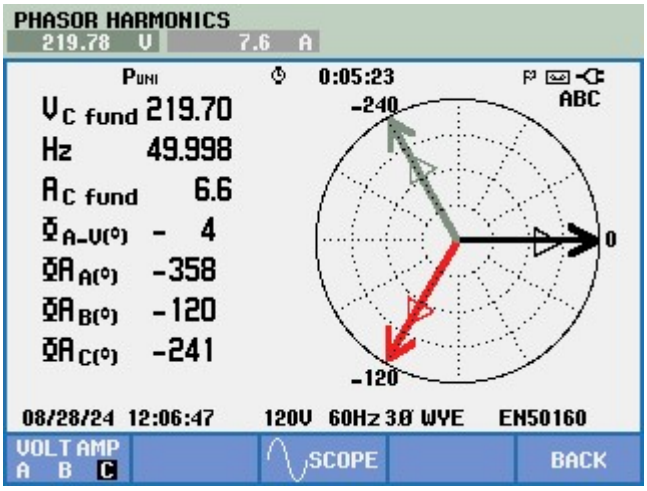


Figure 19. The grid phasor harmonics.

The three-phase bridge diode rectifier behaved as a nonlinear load. Due to the nonlinear load, the current flow in the national grid was strongly distorted (Figure 20). Additionally, the phase grid voltage is shown (Figure 21).

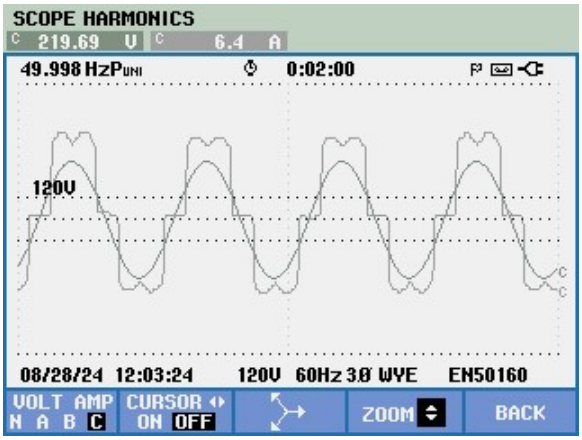


Figure 20. The grid phase voltage and phase current without an SAPF connection.

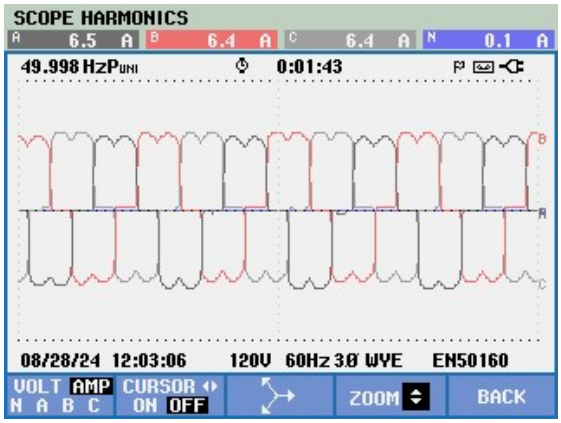


Figure 21. The nonlinear three-phase load current system.

The nonlinear load produced distorted load currents (Figure 19). In Figure 19, the three-phase load currents are shown.

The Power Analyzer measured the harmonics content of the phase load current (Figure 22). It should be noted that there was a high level of current distortion

(THDi = 29.1%). In the OFF operation mode (no APF connection), this load current flowed through the power supply.

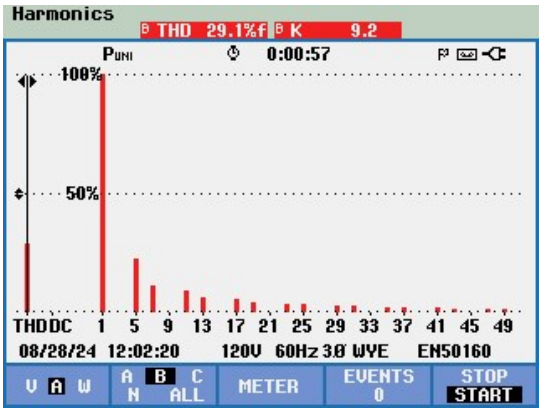


Figure 22. The harmonics content of the load current, THD_i = 29.1%.

At the same time, the harmonic content of the phase current in the power supply was obtained from the Power Analyzer (Figure 23). In the case of the nonlinear load, without any harmonic compensation, a harmonic content of the power supply voltage of THDu = 0.9% was obtained.

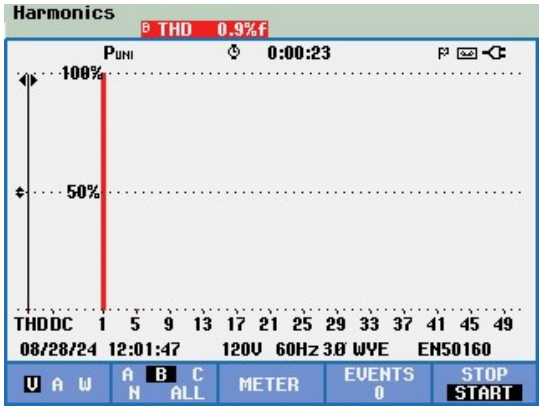


Figure 23. The harmonics content of the power supply voltage, THD_u = 0.9%, without an SAPF connection.

In Figure 24, in the ON operating mode (the SAPF was connected in parallel with the load), the measured three-phase grid voltage system is shown.

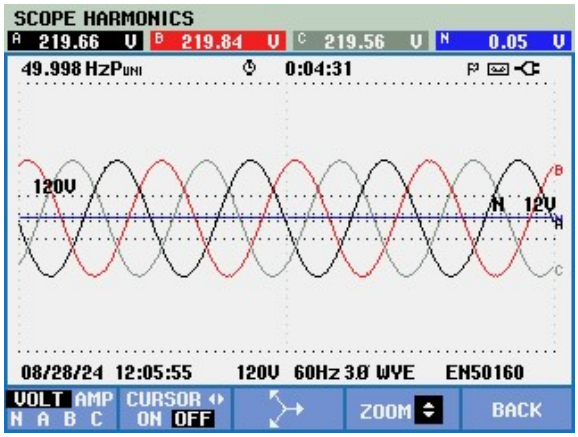


Figure 24. The grid three-phase voltage system with an SAPF connection.

In this operation mode (SAPF connected), the grid current harmonic distortion decreased to THDi = 5.6% (Figure 25).

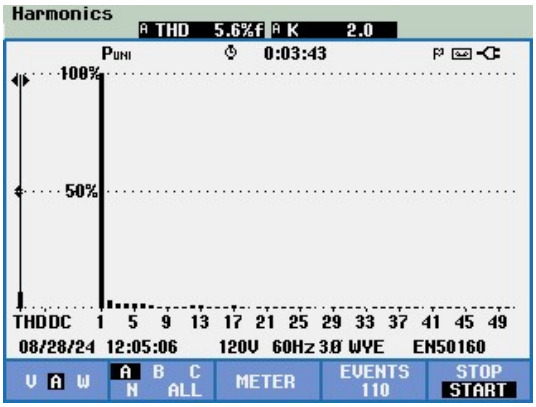


Figure 25. The harmonics content of the grid phase current with an SAPF connection: THD_i = 5.6%.

At the same time, the grid voltage harmonic distortion decreased to THD_u = 0.2% (Figure 26).

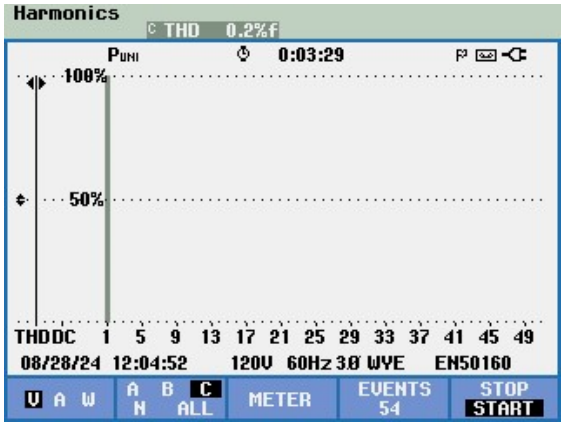


Figure 26. The harmonics content of the grid phase voltage with an SAPF connection: THD_u = 0.2%.

By connecting it to the SAPF, in Figure 27, both the phase current and voltage of the national grid are shown. A qualitative interpretation of the SAPF can be extracted from the above-mentioned figure: the harmonic content of both signals was low, and a near-unity power factor was obtained. A quantitative interpretation can be extracted from the measured experimental data (Table 2).

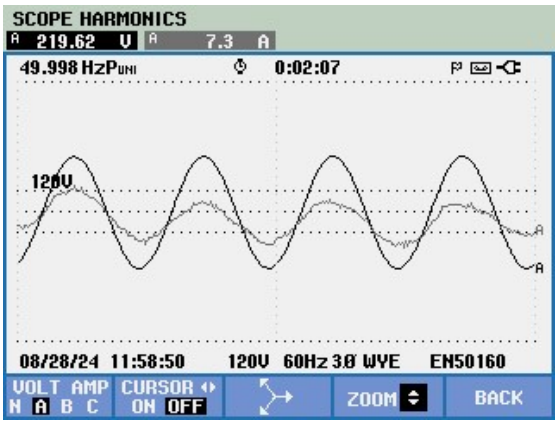


Figure 27. The grid phase voltage and current with an SAPF connection.

Table 2. THD data obtained with rated 220V phase supply voltage.

	Harmonic Level Distortion without SAPF	Harmonic Level Distortion with SAPF
THD_u [%]	0.9	0.2
THD_i [%]	29.1	5.6

According to the obtained experimental data (Table 2), taking into consideration the 220 V grid phase voltage, by connecting the SAPF to the grid, the voltage harmonic level distortion decreased from 0.9% to 0.2%. From a current point of view, by connecting the SAPF to the grid, the grid current harmonic level distortion decreased from 29.1% to 5.6% (Figure 28). Therefore, in Figure 28, the comparative experimental results of the grid current harmonic distortion (without the SAPF and with the SAPF) are presented.

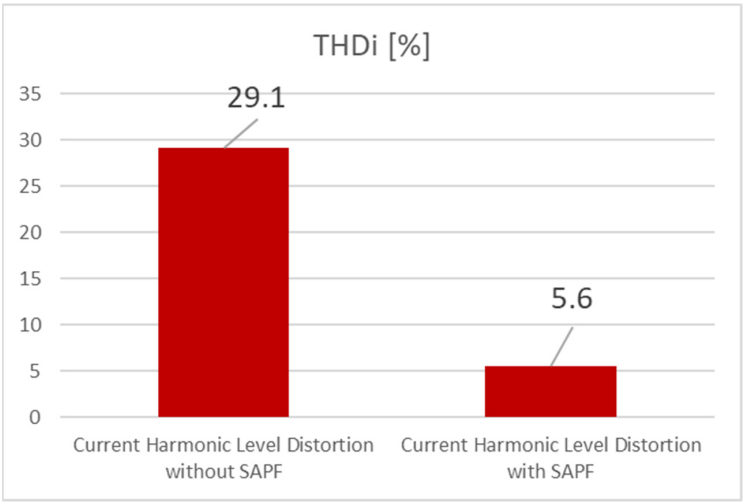


Figure 28. Comparative experimental results of the harmonic distortion (without the SAPF and with the SAPF) for grid current signals.

In Figure 28, the comparative experimental results of the grid voltage harmonic distortion (without the SAPF and with the SAPF) are presented. In Figure 29, the comparative experimental results of the harmonic distortion (without the SAPF and with the SAPF) for grid voltage signals are depicted.

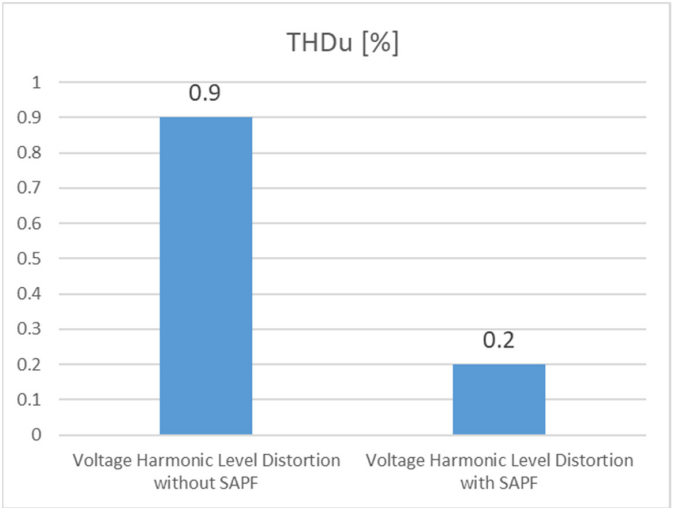


Figure 29. Comparative experimental results of the harmonic distortion (without the SAPF and with the SAPF) for grid voltage signals.

On the front of the SAPF prototype, a programmed touchscreen acts as a Human Machine Interface. By pressing a virtual button on the HMI, the menu of the SAPF prototype can be accessed. In this manner, the main parameters of the APF can be monitored on-line (Figure 30a). On the right side, the Point of Common Coupling is illustrated (Figure 30b). The current and voltage transducers from the Power Analyzer Tool are connected. The SAPF system was tested on balanced loading conditions. For the linear modulation operation $m < 1$ (m, modulation index) for stability purposes, the DC link voltage chosen was greater than 1.63 times the Line-to-Line voltage (V_s), according to the following:

$$V_{dc} > \left(2 \times V_s \times \sqrt{2}\right) \div m \quad (12)$$



(**a**) (**b**)

Figure 30. The Human Machine Interface on the front of the SAPF prototype (**a**) and the Point of Common Coupling (**b**).

Therefore, the constant DC link reference of 690 V_{dc} was set up as a constant on the FPGA control side [31].

The three-phase shunt active power filter system is characterized by a flexible structure in terms of the grid voltage and frequency and can be used for the design and testing of active power filters for any worldwide three-phase low-voltage power supply system (the European Union, United States of America, Japan, Australia, etc.) [32]. The SAPF is characterized by the implementation of the control algorithm on an FPGA-type processor, with the parallel execution of the control loops. The designed control loops were tested successfully on the industrial prototype [32]. In Table 3 the main parameters of the power system are provided.

Table 3. The parameters of the power system.

Power System	Parameter	Rated Value	SI Units
Power grid	Line voltage (V_s)	380	V
	Grid frequency	50	Hz
Nonlinear load	Resistance (R)	11.75	Ω
Shunt active power filter	Inductance (L)	0.00356	H
	DC link capacitance (C)	0.0047	F
	Switching frequency (f_{sw})	15,000	Hz
	DC link voltage (V_{dc})	690	V
DC link voltage controller	Proportional gain (k_p)	1.3	
	Integral coefficient (k_i)	30	

5. Conclusions

These results are part of the "Knowledge Transfer Regarding the Energy Efficiency Increase and Intelligent Power Systems" project co-funded by the European Union from the European Regional Development Fund through the Competitiveness Operational Program 2014–2020. The authors of this paper present the Harmonic Component Separation Method with a Low-Pass Filter Control applied in the field of power quality on the industrial prototype. The delivered technical parameters are in accordance with the EN 61000-6-2, EN 61000-6-4 and EN 50178 standards. The conception of the SAPF control took into consideration harmonics extraction from the load currents based on the LPF method. The designed control loops were tested successfully, the implemented method was described in detail in the present research work and both numerical and experimental results were delivered. The SAPF prototype is characterized by the implementation of the control algorithm on an FPGA-type processor, with the parallel execution of the control loops. The provided experimental results confirm a power quality improvement on the grid side in a harmonic-polluted power system supplying a three-phase nonlinear load. The current harmonic content on the source side was reduced to THD_i = 5.6% (Figure 28). Additionally, the voltage harmonic content was reduced to THD_u = 0.2% (Figure 29). Therefore, the solution is efficient in a three-phase balanced system with balanced loads. The delivered results of the laboratory tests demonstrate the feasibility of implementing the control in the industrial prototype. This first step catalyzes SAPF line production in the industrial area through the unitary and efficient integration of all the specific actors (enterprises, research institutes, universities and entrepreneurs) in innovation.

Author Contributions: Conceptualization, M.G. and S.E.; methodology, M.G.; software, M.G. and S.E.; validation, M.G., S.E. and R.C.S.; formal analysis, M.G.; investigation, R.B.; resources, M.G., S.E., R.B. and R.C.S.; data curation, M.G. and S.E.; writing—original draft preparation, M.G.; writing—review and editing, M.G., S.E., R.B. and R.C.S.; visualization, M.G.; supervision, M.G.; project administration, M.G.; funding acquisition, M.G. All authors have read and agreed to the published version of the manuscript.

Funding: This research received no external funding.

Data Availability Statement: The original contributions presented are included in this article; further inquiries can be directed to the corresponding author.

Acknowledgments: This study was supported by the CRESC INTEL project "Knowledge Transfer Regarding the Energy Efficiency Increase and Intelligent Power Systems", ID/Cod My SMIS: P_40_340/105803, project co-funded by the European Union from the European Regional Development Fund through the Competitiveness Operational Program 2014–2020.

Conflicts of Interest: The authors declare no conflicts of interest.

Abbreviations

APF	Active power filter
FPGA	Field-programmable gate array
HCSLPF	Harmonic Component Separation Method with a Low–Pass Filter
HMI	Human Machine Interface
LPF	Low-pass filter
PCC	Point of Common Coupling
PLL	Phase-locked loop
PWM	Pulse width modulation
SAPF	Shunt active power filter
THD	Total harmonic distortion

References

1. Veronezi, D.; Soulier, M.; Kocsis, T. Energy Solutions for Decarbonization of Industrial Heat Processes. *Energies* **2024**, *17*, 5728. [CrossRef]
2. Wang, Z.; Dou, Z.; Liu, Y.; Guo, J.; Zhao, J.; Yin, W. Research on Microgrid Optimal Scheduling Based on an Improved Honey Badger Algorithm. *Electronics* **2024**, *13*, 4491. [CrossRef]
3. Liu, X.; Liu, X.; Li, L.; Xu, R.; Ban, Q.; Xu, R. Has Trade Liberalization Promoted Energy Efficiency in Enterprises? *Sustainability* **2024**, *16*, 9826. [CrossRef]
4. Song, W.; Cao, X.; Jiang, H.; Li, Z.; Gao, R. Two-Stage Combined Model for Short-Term Electricity Forecasting in Ports. *Information* **2024**, *15*, 715. [CrossRef]
5. Vizitiu, R.; Vizitiu, Ș.; Burlacu, A.; Abid, C.; Balan, M.; Kaba, N. Experimental Investigation of a Water–Air Heat Recovery System. *Sustainability* **2024**, *16*, 7686. [CrossRef]
6. Han, J.; Feng, B.; Chen, Z.; Liang, Z.; Chen, Y.; Liang, X. Simulation and Application of a New Type of Energy-Saving Steel Claw for Aluminum Electrolysis Cells. *Sustainability* **2024**, *16*, 8061. [CrossRef]
7. Xu, H.; Zhang, N.; Li, Z.; Zhuo, Z.; Zhang, Y.; Zhang, Y.; Ding, H. Energy-Saving Speed Planning for Electric Vehicles Based on RHRL in Car following Scenarios. *Sustainability* **2023**, *15*, 15947. [CrossRef]
8. Šolić, A.; Jakus, D.; Vasilj, J.; Jolevski, D. Electric Vehicle Charging Station Power Supply Optimization with V2X Capabilities Based on Mixed-Integer Linear Programming. *Sustainability* **2023**, *15*, 16073. [CrossRef]
9. Hussan, M.; Sarwar, M.; Sarwar, A.; Tariq, M.; Ahmad, S.; Shah Noor Mohamed, A.; Khan, I.; Ali Khan, M. Aquila Optimization Based Harmonic Elimination in a Modified H-Bridge Inverter. *Sustainability* **2022**, *14*, 929. [CrossRef]
10. Prashant; Siddiqui, A.S.; Sarwar, M.; Althobaiti, A.; Ghoneim, S.S.M. Optimal Location and Sizing of Distributed Generators in Power System Network with Power Quality Enhancement Using Fuzzy Logic Controlled D-STATCOM. *Sustainability* **2022**, *14*, 3305. [CrossRef]
11. Rao, S.; Kumar, Y.; Pradeep, D.; Reddy, C.; Flah, A.; Kraiem, H.; Al-Asad, J. Power Quality Improvement in Renewable-Energy-Based Microgrid Clusters Using Fuzzy Space Vector PWM Controlled Inverter. *Sustainability* **2022**, *14*, 4663. [CrossRef]
12. Kumar, Y.; Rao, S.; Padma, K.; Reddy, C.; Pradeep, D.; Flah, A.; Kraiem, H.; Jasiński, M.; Nikolovski, S. Fuzzy Hysteresis Current Controller for Power Quality Enhancement in Renewable Energy Integrated Clusters. *Sustainability* **2022**, *14*, 4851. [CrossRef]
13. Ahmed, M.; Kandil, T.; Ahmed, E. Enhancing Doubly Fed Induction Generator Low-Voltage Ride-through Capability Using Dynamic Voltage Restorer with Adaptive Noise Cancellation Technique. *Sustainability* **2022**, *14*, 859. [CrossRef]
14. Alghaythi, M.; Irudayaraj, G.; Ramu, S.; Govindaraj, P.; Vairavasundaram, I. Mathematical Modeling and Analysis of Capacitor Voltage Balancing for Power Converters with Fewer Switches. *Sustainability* **2023**, *15*, 10698. [CrossRef]
15. Nyamathulla, S.; Chittathuru, D. A Review of Multilevel Inverter Topologies for Grid-Connected Sustainable Solar Photovoltaic Systems. *Sustainability* **2023**, *15*, 13376. [CrossRef]
16. Hoffmann, S.; Bock, M.; Hoene, E. A New Filter Concept for High Pulse-Frequency 3-Phase AFE Motor Drives. *Energies* **2021**, *14*, 2814. [CrossRef]
17. Ertasgin, G.; Whaley, D. Analysis and Optimization of Output Low-Pass Filter for Current-Source Single-Phase Grid-*Connected* PV Inverters. *Appl. Sci.* **2024**, *14*, 10131. [CrossRef]
18. Rameshkumar, T.; Chandrasekar, P.; Kannadasan, R.; Thiyagarajan, V.; Alsharif, M.; Kim, J. Electrical and Mechanical Characteristics Assessment of Wind Turbine System Employing Acoustic Sensors and Matrix Converter. *Sustainability* **2022**, *14*, 4404. [CrossRef]
19. Anjum, W.; Husain, A.; Abdul Aziz, J.; Fasih ur Rehman, S.; Bakht, M.; Alqaraghuli, H. A Robust Dynamic Control Strategy for Standalone PV System under Variable Load and Environmental Conditions. *Sustainability* **2022**, *14*, 4601. [CrossRef]
20. Akagi, H. New trends in active filters for improving power quality. In Proceedings of the International Conference on Power Electronics, Drives and Energy Systems for Industrial Growth, New Delhi, India, 8–11 January 1996; Volume 1, pp. 417–442. [CrossRef]
21. Iqbal, M.N.; Baliarsingh, A.K.; Puhan, P.S. Power Quality Improvement using a Novel Controller in Shunt Active Power Filter. In Proceedings of the 2024 1st International Conference on Cognitive, Green and Ubiquitous Computing (IC-CGU), Bhubaneswar, India, 1–2 March 2024; pp. 1–5. [CrossRef]
22. Ionescu, F.; Six, J.P.; Floricau, D.; Delarue; Nitu, S.; Bogus, C. *Electronica de Putere. Convertoare statice (Power Electronics. Static Converters)*; Editura Tehnica: Bucuresti, Romania, 1998.
23. *EN IEC 61000-6-2:2019*; Electromagnetic Compatibility (EMC)—Part 6-2: Generic Standards—Immunity Standard for Industrial Environments. International Electrotechnical Commission: Geneva, Switzerland, 2019.
24. *EN IEC 61000-6-4:2019*; Electromagnetic Compatibility (EMC)—Part 6-4: Generic Standards—Emission Standard for Industrial Environments. International Electrotechnical Commission: Geneva, Switzerland, 2019.
25. *EN 50178:1997*; Electronic Equipment for Use in Power Installations. European Standard: Brussels, Belgium, 1997.

26. Hoff, B.; Sulkowski, W. A simple DC-link pre-charging method for three-phase voltage source inverters. In Proceedings of the IECON 2012—38th Annual Conference on IEEE Industrial Electronics Society, Montreal, QC, Canada, 25–28 October 2012. [CrossRef]
27. Schnetzka, H.R. System for Precharging a DC Link in a Variable Speed Drive. U.S. Patent US7619906B2, 7 July 2009.
28. Ozguc, M.K.; Ipek, E.; Aras, K.; Erhan, K. Comprehensive Analysis of Pre-Charge Sequence in Automotive Battery Systems. *Trans. Environ. Electr. Eng.* **2019**, *4*, 1–6. [CrossRef]
29. Bose, B.K. An adaptive hysteresis-band current control technique of a voltage-fed PWM inverter for machine drive system. *IEEE Trans. Ind. Electron.* **1990**, *37*, 402–408. [CrossRef]
30. Gupta, N.; Singh, S.P.; Dubey, S.P. DSP based adaptive hysteresis-band current controlled active filter for power quality conditioning under non-sinusoidal supply voltages. *Int. J. Eng. Sci. Technol.* **2011**, *3*, 236–252. [CrossRef]
31. Kumar, R.; Bansal, H.O. Hardware in the loop implementation of wavelet based strategy in shunt active power filter to mitigate power quality issues. *Electr. Power Syst. Res.* **2019**, *169*, 92–104. [CrossRef]
32. Marian, G.; Ionut, E.S.; Constantin, S.R.; Razvan, B. Unification of the Implementation and Testing of Control Algorithms for Three-Phase, Low-Voltage, Parallel-Type Active Power Filters, in Experimental Stand and in Prototypes, Active Power Filters. Patent 137988 A2, 25 August 2022.

Disclaimer/Publisher's Note: The statements, opinions and data contained in all publications are solely those of the individual author(s) and contributor(s) and not of MDPI and/or the editor(s). MDPI and/or the editor(s) disclaim responsibility for any injury to people or property resulting from any ideas, methods, instructions or products referred to in the content.